Bull. Astr. Soc. India (1982) 10, 1-15

Multi-station observations of interplanetary scintillations

S. Ananthakrishnan *Radio Astronomy Centre, Tata Institute of Fundamental Research, Ootacamund 643 001*

J. J. Kaufman *Department of Electrical Engineering and Computer Sciences, University of California, San Diego, La Jolla, California 92093, USA*

Received 1981 December 30

Abstract. Solar wind velocity estimation using the method of multi-station interplanetary scintillation observations has been reviewed. It is shown that the inferred model for the electron density fluctuations in the solar wind differs significantly from that for the proton density. The high latitude solar wind has a strong correlation with the presence of coronal hole regions.

Key words : solar wind—intensity scintillation—coronal holes

1. Introduction

The earliest arguments for the existence of an ubiquitous interplanetary 'wind' orginating in the sun were proffered by comet specialists. Their evidence was the observation that an ionic comet tail invariably pointed away from the sun, regardless of the comet's direction of motion. Since radiation pressure was deemed insufficient to explain this anomaly, it was argued that some unseen and previously unknown mechanism must be at work. Today we call this phenomenon the solar wind.

The first viable theory of the solar wind was proposed by Parker (1958). He showed that a wind expanding at hundreds of kilometers per second was the natural consequence of the million-degree temperature in a corona bound by the sun's gravitational field. The temperature, furthermore, would decrease very slowly with distance from the sun, thus ensuring a fully ionized wind in the interplanetary space.

It was soon pointed out that the free electrons would scatter radio waves propagating through the interplanetary medium. A similar effect was known to occur in the earth's ionosphere, where variations in the electron density cause the signals from most celestial radio sources to fluctuate randomly, or 'scintillate'. The phenomenon is analogous to the twinkling of starlight, which is caused by turbulence in the neutral atmosphere.

In the early 1960s the existence of the solar wind was proven by observations from spacecraft, and Hewish *et al.*, (1964) announced the discovery of interplanetary scintillations of radio sources. It was quickly realized that scintillations could be used to measure the solar wind velocity if they were observed at several suitably spaced stations. The first such measurements were reported by investigators in Britain (Dennison & Hewish 1967); subsequently three-station observatories were established in the U.S.S.R. (Vitkevitch & Vlasov 1970), the U.S.A. (Armstrong & Coles 1972) (figure 1a) and Japan (Watanabe *et al.* 1973). More recently a similar three-station system is being constructed by the Physical Research Laboratory, Ahmedabad, with baseline separations of about 200 km and operating at 103 MHz (Alurkar & Bhonsle 1980).

In this paper we discuss the kinds of information which can be extracted from multi-station observations of interplanetary scintillations (called for brevity 'IPS'). IPS has been used not only to investigate the solar wind but also to study radio source structure as well. But since three-station systems usually consist of only small or medium sized antennas it is not possible to get structural information on a large number of sources. This is better obtained with large single instruments like the Ooty radio telescope or the Cambridge IPS array. However, valuable results have been obtained on a few sources (*e.g.* Coles & Kaufman 1977). In what follows, we first introduce the intensity correlation function and spectrum and describe ways to estimate the solar wind velocity and source structure from these. Later we describe in brief how, by a comparison between the velocities estimated from IPS and those measured *in situ* by spacecraft, we may obtain useful information on the nature of the electron density fluctuations and their possible relation to the physics of the solar wind turbulence. We also discuss how the IPS velocity data are being used to construct a 3-dimensional picture of the solar wind.

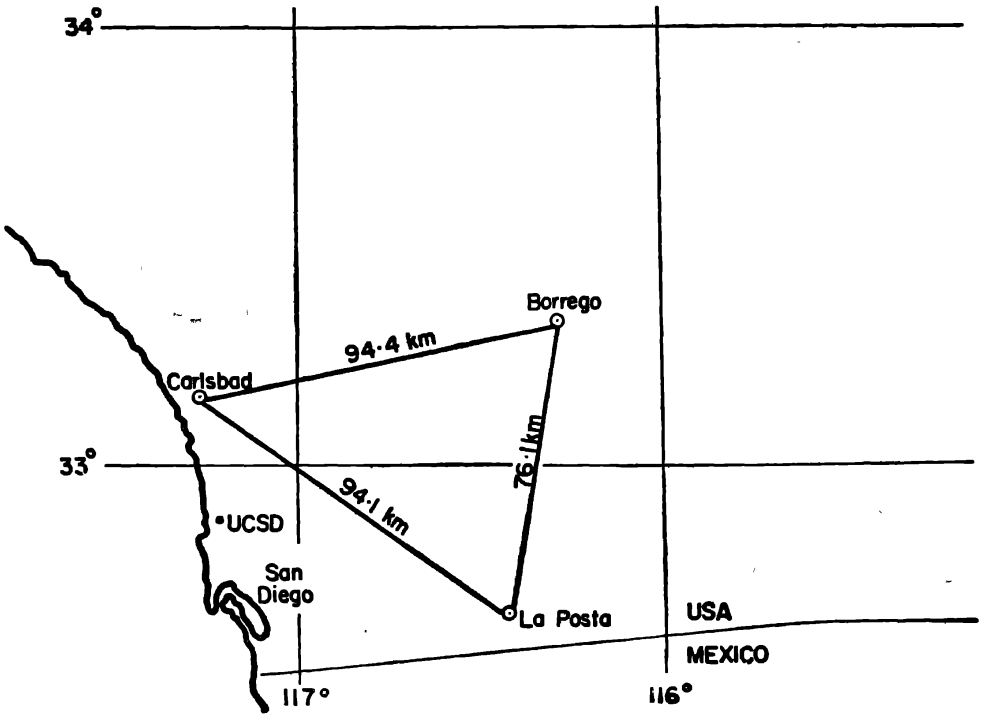

Figure 1a. Typical geometry of an IPS 3-station system.

2. The intensity correlation function

When a compact radio source is observed through the solar wind, the refractive index variations in the wind cause fluctuations in both the phase and the amplitude of the electric field induced at the antenna. The systems we will discuss, however, measure only the intensity of the signal. A time series of intensity scintillations is shown in figure 1b. Most of the peaks in the intensity are seen to appear at the three radio telescopes at distinctly different times. This is evidence for a moving diffraction pattern. One needs to know only the separations of the antennas to estimate the solar wind velocity from these offsets. In fact this method—called the 'similarity method'—was used in the earliest IPS velocity measurements.

In most observations, however, the signal-to-noise is insufficient to yield reliable velocity estimates from the similarity method. Furthermore, the measured 'velocity' may vary from feature to feature because the pattern of refractive index irregularities is slowly rearranging itself. These difficulties may be overcome by using such statistical tools as the correlation function and the spectrum. We will discuss the correlation function first.

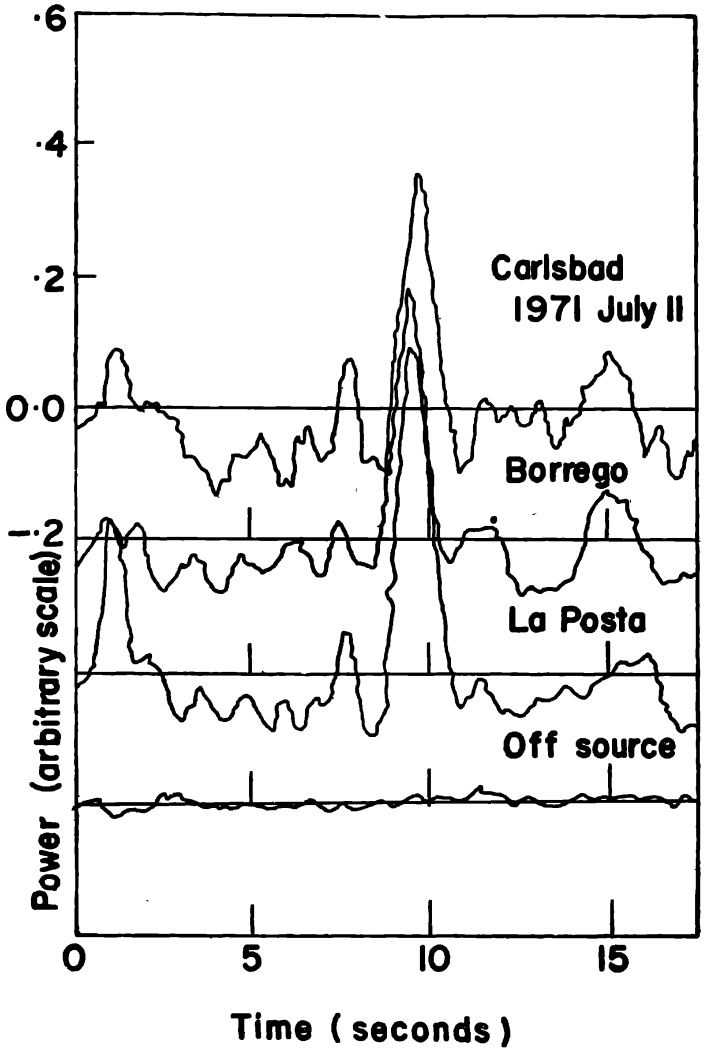

Figure 1b. IPS time series observed on 3C144. Station geometry is such that an IPS 'spike' is first observed at Borrego and La Posta and then about 0.2 s later at Carlsbad (Armstrong 1975).

The intensity correlation function $\rho(\bar{r}, \tau)$ which defines the correlation at a time lag τ between two time series of intensity measured at stations separated by a baseline $\bar{r} = (x, y)$ is given by

$$\rho(r, \tau) = \langle I(\bar{r}_0, t_0)\, I(\bar{r}_0 + \bar{r}, t_0 + \tau)\rangle / \langle I^2 \rangle, \qquad ...(1)$$

where $I(\bar{r}, t)$ is the intensity deviation from the mean and the angular brackets denote averaging over space and time. The averaging smooths out the random variations and makes it possible to formulate a well-defined description of the structure and dynamics of the scintillation pattern. For an accurate normalization of $\rho(\bar{r}, \tau)$ a good estimate of $\langle I^2 \rangle$ is required, but due to contamination by interference and ionospheric scintillation the normalization is rarely accurate to better than 10 per cent.

In a real observing system the measured correlation function provides a complete picture of the variation of the scintillations with time τ, but not with separation $\bar{r}$. This is because typically there are only three stations in the system, giving three baselines. Under certain conditions, however, the temporal and spatial variations are essentially identical. In this case the scintillation pattern is said to be frozen; that is, the refractive index irregularities are thought of as being convected rigidly at a uniform velocity, υ, through space. The correlation function is then obtained by Galilean transformation $x \to x - \upsilon_x \tau$, $y \to y - \upsilon_y \tau$ so that

$$\rho(\bar{r}, \tau) = \rho(\bar{r} - \bar{\upsilon}\tau), \qquad ...(2)$$

which maximizes at a time

$$\tau_p = \frac{\bar{r} \cdot \bar{\upsilon}}{\upsilon^2} = \frac{x\upsilon_x + y\upsilon_y}{\upsilon^2}, \qquad ...(3)$$

where x and y are the spatial coordinates and υ_x, υ_y are component velocities in the x, y directions. If there are two or more baselines (that is, at least three observing stations), both the magnitude and direction of $\bar{\upsilon}$ can be determined using measurements of τ_p from any two or more correlation functions.

2.1 *The midpoint velocity*

The simple model discussed above assumes that the velocity is unique. But with a scattering medium as extensive as the solar wind, this is of course only an approximation. As shown in figure 2, scattering occurs all along the line of sight to the source. Unless the turbulence is very strong, however, there is no multiple scattering at metre wavelengths, so that the contributions to the scintillation pattern from different regions are independent. Each region produces its own scintillation pattern, which drifts at the velocity characteristic of that region. Only the velocity component perpendicular to the line of sight is seen by the antenna system; so even if the wind has the same velocity everywhere the effective pattern velocity will be different from region to region. In fact, the solar wind is never uniform in space; transient disturbances (from solar flares, for instance) and long-lived solar wind streams from coronal holes cause large spatial variations. Velocities range from 200 to 1000 km s^{-1}, and

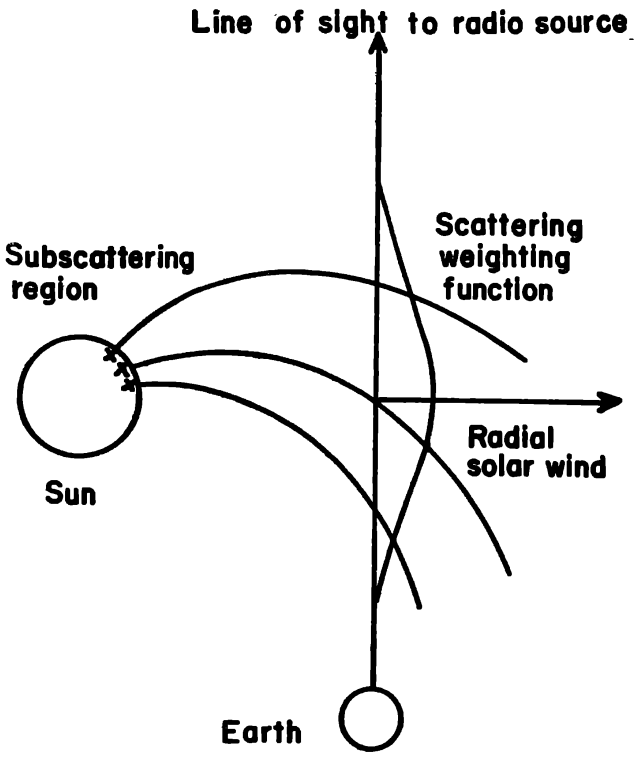

Figure 2. The geometry of an IPS observation showing the line of sight, the scattering weighing function and the region on the sun from which the solar wind is taken to have come (Sime 1976).

spacecraft have observed the velocity at the leading edge of a stream to double in a matter of hours.

Each region along the line of sight adds its contribution to the final scintillation pattern, but it is a weighted sum. The average weighting or scattering function, as it is called, varies as the square of the average electron density; that is, it varies as r^{-4} with distance from the sun. Thus the scattering is strongest where the line of sight passes closest to the sun, and consequently the velocities in that region are most strongly reflected in the motion of the scintillation pattern.

In general the effect of multiple velocities is to produce a 'skewed' cross correlation function in which the midpoint of the function at a specified fraction of the function's maximum value moves monotonically away from τ_p as the height at which it is measured decreases. (If the velocity is unique, of course, the correlation function is symmetric, and the midpoint at any height is τ_p.) A typical skewed correlation function can be constructed by superimposing two (or more) symmetric correlations having the same spatial scale but different velocities. The two functions have the same height at $\tau = 0$ (since the spatial scale is all that matters there), but the high velocity function is narrow and peaks closer to $\tau = 0$ than the low velocity function which is broad. If the two are added, the resulting function rises rapidly to its peak (which occurs between the peaks of the two component functions, but closer to the peak of the high velocity one), then decays slowly, producing a skew in the direction of increasing $|\tau|$.

In IPS observations, skewed correlation function is the rule rather than the exception. Consequently the problem facing the investigator, stated generally, is to infer

what he can about the distribution of the velocities. It is possible, of course, to fit the correlation functions with extensive models that include an assumed form for the velocity distribution (*e.g.* Little & Ekers 1971). However, such attempts are generally more effort than they are worth, since they are very sensitive to small errors in normalizing the correlation functions.

A different approach is to use the skewness of the correlation function directly to define a series of velocity estimates based on the midpoints at various heights. for example, if $\tau_{m_{50}}$ is the midpoint at 50 per cent of the correlation function's maximum, then $\upsilon_{m_{50}}$ is derived by solving $\tau_{m_{50}} = \bar{r}.\bar{\upsilon}_{m_{50}}/\upsilon^2_{m_{50}}$ in precisely the same way as the peak velocity is obtained from τ_p. The midpoint velocities can be used to estimate such statistical properties of the velocity distribution as its mean. Strictly speaking, different velocity distributions require different midpoint velocity estimators for the mean, but investigators usually adopt a single estimator for the sake of consistency. The American IPS group uses $\upsilon_{m_{50}}$ (Coles & Maagoe 1972; Coles & Kaufman 1978), while the Japanese group uses a weighted average of the midpoint velocities between 50 and 90 per cent of the maximum. The peak velocity is biased toward the high end of the distribution, so the difference between υ_p and, say, $\upsilon_{m_{50}}$ gives an idea of its range. In short, the midpoint velocities provide distribution parameters that are simply calculated and stable in the presence of noise, and that is why they have been used extensively.

3. The frequency spectrum

So far we have discussed only the time statistics of an IPS observation, but we will now consider the frequency domain. Define the intensity spectrum $\Phi(f)$ as

$$\Phi(f) = \frac{1}{2\pi}\int_{-\infty}^{\infty} d\tau \rho(\tau) \exp(-2\pi i f\tau), \qquad ...(4)$$

that is, as the Fourier transform of the correlation function. This equation is useful in showing the relation between $\Phi(f)$ and $\rho(\tau)$, but in practice the spectrum is usually calculated first because averaging, filtering, noise removal, and error estimation are more conveniently performed in the frequency domain. Note that the solar wind velocity can be estimated from the cross-spectrum of intensity measurements from two antennas just as it can be derived from the cross-correlation function. If the latter is $\rho(\bar{r} - \bar{\upsilon}\tau)$, its transform is $\Phi_{\bar{r}}(f) = \Phi_0(f)\ e^{-2\pi i f \bar{r}.\bar{v}/v^2}$. The slope of the phase of $\Phi_{\bar{r}}(f)$ is $\bar{r}.\bar{\upsilon}/\upsilon^2$, which is of course the same as τ_p of equation (3). An example of the cross-spectral phase is shown in figure 3. Here the phase is unusually linear, indicating the dominance of a single velocity. When a range of velocities is present, on the other hand, the phase is curved. By modelling the dependence of the shape of the phase curve on the underlying velocity distribution, one can estimate the distribution parameters.

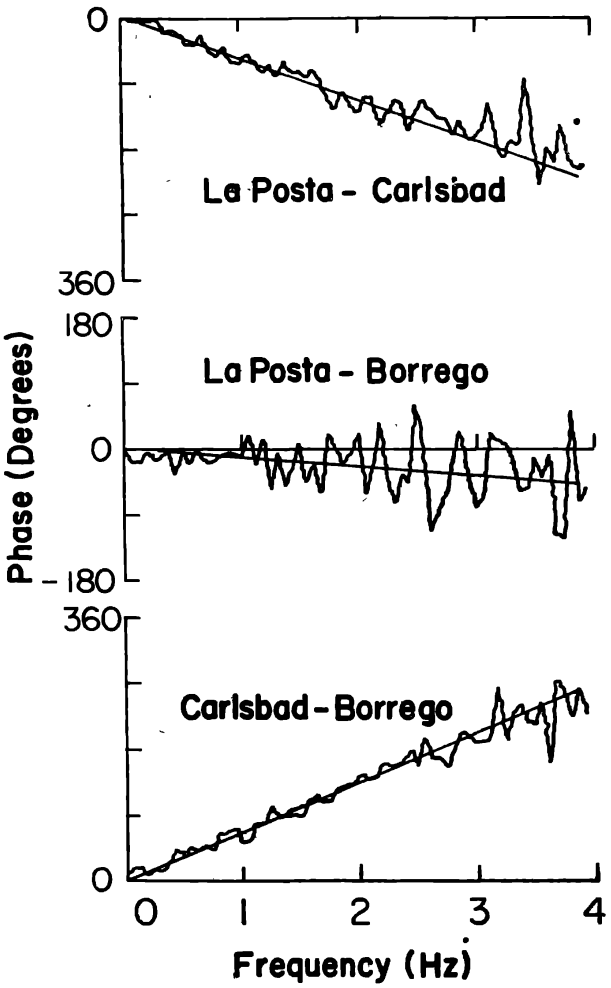

Figure 3. Cross spectral phase for 3C144 on a day when a single velocity is dominant (Kaufman 1976).

3.1 *A physical interpretation of the spectrum*

In many respects the physics of IPS is clearer in the frequency domain than in the time domain. This is so because in the spectrum the diverse effects of the electron irregularity spectrum, the source, and the diffraction 'filter' are multiplicative rather than convolutional, as they are in the correlation function. In this discussion we will restrict ourselves to 'weak' scattering, where the theory is complete and well-understood. In weak scattering the r.m.s. phase deviation, ϕ_0, across the wavefront characterizing the strength of scattering in the solar wind medium is very small and mean squared phase deviation $\phi_0^2 \ll 1$. Actually, the term 'weak' scattering is less restrictive than it sounds. Most metre wavelength observations are made in weak scattering, and indeed a completely satisfactory interpretation of the commonly used velocity estimators under conditions of strong scatering has never been presented.

First we discuss the limiting case of a point source whose signal is incident upon a thin screen of stationary, 'frozen' scattering medium. The spatial spectrum of intensity at a distance z from the screen is given by

$$\Phi_{I_{pt}}(\kappa_x, \kappa_y) \propto \Phi_{n_e}(\kappa_x, \kappa_y) \sin^2 \left[z\left(\frac{\kappa_x^2 + \kappa_y^2}{2k} \right) \right], \quad \ldots(5)$$

where Φ_{n_e} is the spatial spectrum of electron density irregularities, κ is the spatial frequency, and $k = 2\pi/\lambda$ for a signal of wavelengh λ. The sin term, called the 'Fresnel filter', embodies the diffraction effects, showing that certain spatial frequencies are enhanced and others inhibited by the interference of the scattered waves with each other.

The irregularity spectrum Φ_{n_e}—which contains information about the physics of turbulence in the solar wind—is a subject of continual study. Its functional form has never been conclusively established, although the current consensus is that Φ_{n_e} is best modelled as a power law with one or more breaks in it (Coles 1978; Woo & Armstrong 1979). The power law indices most often mentioned are between 3 and 4. The Cambridge group however continues to favour a Gaussian model as the best fit for the spectrum (Readhead *et al.* 1978). In reality the spectrum appears to be more complex than any commonly used model; furthermore, it varies with distance from the sun and with the passage of high speed streams and energetic transients.

Equation (5) gives a 2-dimensional spatial spectrum, $\Phi_{I_{pt}}(\kappa_x, \kappa_y)$. In an IPS experiment, however, the signal is a time series, giving a temporal spectrum, $\Phi_{I_{pt}}(f)$. The two are related by

$$\Phi_{I_{pt}}(f) = \int_{-\infty}^{\infty} d\kappa_y \; \Phi_{I_{pt}}\left(\kappa_x = \frac{2\pi f}{\upsilon}, \kappa_y \right) \quad \ldots(6)$$

for the case where the velocity is in the x-direction. Thus spatial variations of order κ^{-1} are detected as temporal variations of order $(\upsilon\kappa)^{-1}$.

We now generalize these point source results to the case of an extended source. An extended souce can be considered as an ensemble of point sources which produce identical scintillation patterns that are slightly offset from each other, causing a 'blurring' effect. Mathematically the extended source acts as a low pass filter on the point source spectrum, cutting off the high frequency fluctuations:

$$\Phi_{I_{\text{extended}}} = | V(\kappa_x z, \kappa_y z) |^2 \Phi_{I_{pt}}. \quad \ldots(7)$$

Here V is the source visibility function, the Fourier transform of its angular brightness distribution. The broader the source, the narrower the visibility, and the stronger the effect on the spectrum.

3.2 *Source diameter measurements*

As the source moves closer to the sun, the strength of scattering increases and the point source spectrum broadens. At some point it becomes sufficiently broad that the shape of the intensity spectrum is precisely that of the source visibility function. The half power angular diameter of the source, θ, can then be obtained from (Cohen 1969)

$$\theta \approx c\upsilon/f_2 z,$$

where f_2 is the width of the temporal spectrum, υ the velocity, z the distance to the scattering region, and c a constant which depends on the functional form of the brightness distribution. Figure 4 shows two source-limited spectra, along with weak scattering spectra for the same source. The dashed lines show model spectra for a much larger source, which is barely distinguishable from the small source in weak scattering. Also, since the width of the spectrum is sensitive to the position angle of the solar wind across the source, by observing the spectral width at different position angles it is possible to deduce the two dimensional structure of compact scintillating sources. Structure of a large number of sources has been derived this way (Ananthakrishnan 1976; Swarup 1977).

The success of the above methods for measuring source diameters depends on the accuracy to which the velocity is known. (The distance to the dominant scattering region is ordinarily assumed to be the distance to the point of closest approach of the line of sight to the sun, a very good assumption for observations close to the sun). If the velocity is not available—say, because the data are from single-station measurements—a 'typical' velocity must be assumed The method is risky if there is only one observation, but it can be used with more confidence if many observations are averaged together.

The IPS methods for measuring source structure cannot compete with interferometry methods at high observing frequencies, but they are important at low frequencies (around 100 MHz). To see why, consider the angular resolution of the two methods. The interferometry resolution is $\Delta\theta = \lambda/d$, where d is the baseline and λ the observing wavelength; the IPS resolution is $\Delta\theta = \upsilon/(f_0 z)$, where f_0 is the largest temporal frequency observed in the intensity fluctuations. To measure a 0.2 arcsec source at $\lambda = 4$ m with interferometry requires a baseline of roughly 4000 km; for $z = 1$ AU and $\upsilon = 400$ km s^{-1}, IPS achieves the same resolution at $f_0 = 3$ Hz, and this is independent of the observing frequency. In interferometry such angular resolution can be realized in very long beseline interferometry (VLBI) experiments, but so far there have been few low frequency studies. On the other hand, IPS observations out to frequencies of 3 Hz or greater are routine. Thus they are likely to continue to provide the only low frequency data available on the structure of many compact objects.

4. Anisotropic scintillation patterns

In weak scattering, source structure effects are less dramatic, but nevertheless noticeable if the source is strongly noncircular. An elliptical or double source, for example, can cause the scintillation correlation pattern to be elliptical, in a statistical sense—that is, it produces a correlation function in which contours of equal correlation are elliptical. If care is not taken when analyzing such correlation functions, the velocities derived from them will be biased because of the unrecognized anisotropy. But if either the actual direction of velocity flow or the anisotropy of the pattern is known, an unbiased estimate of the velocity magnitude can be made. From a knowledge of the systematic effects produced by pattern anisotropy also it is possible to determine, in case of some strong sources, a measure of their source structure in different position angles. These results are described by Kaufman (1976) and Coles & Kaufman (1978).

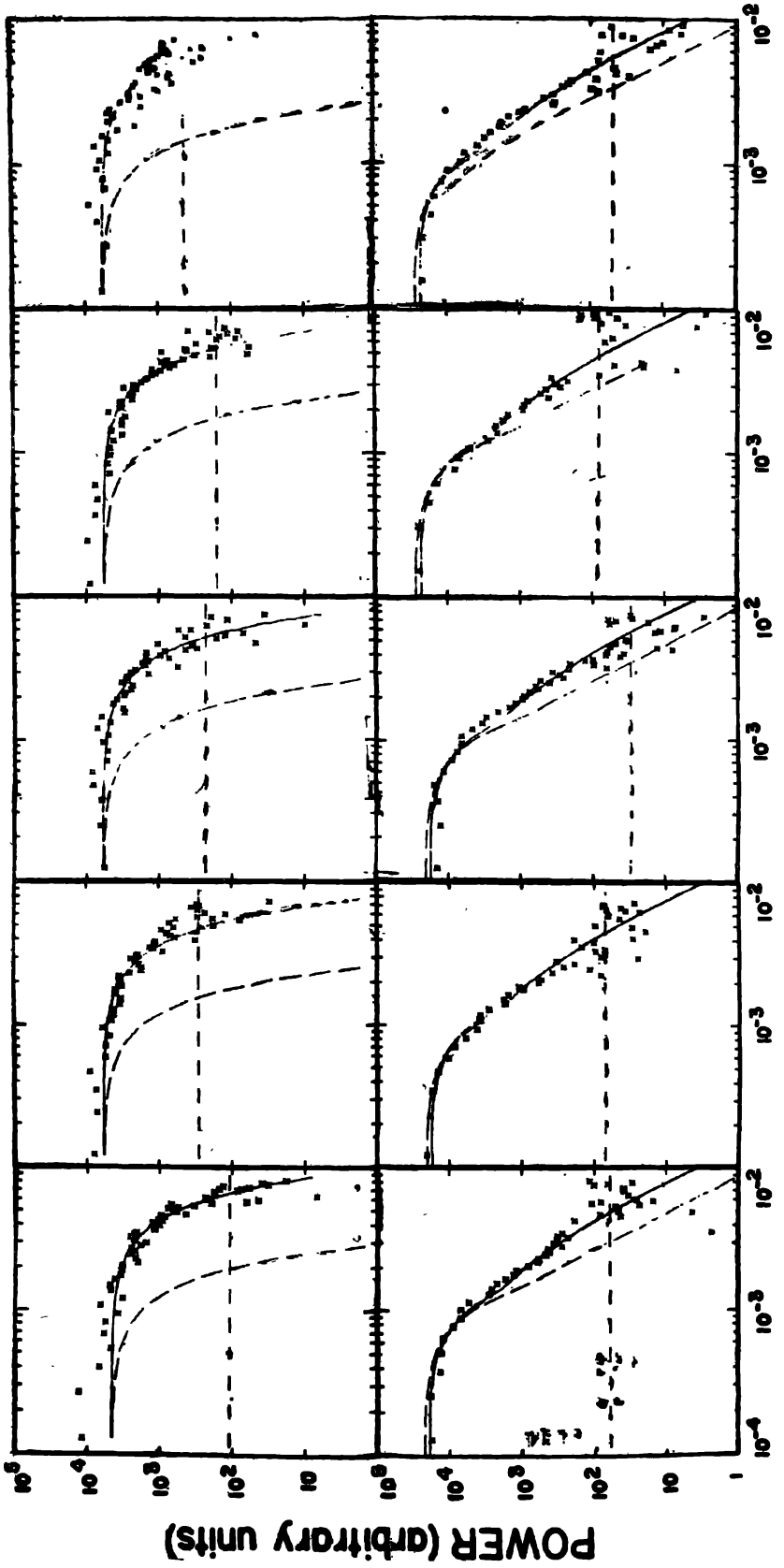

Figure 4. Intensity spectra at 74 MHz for the Crab pulsar for the years 1972–76 from left to right. Top row : Strong scattering spectra for elongations 15–20°. Solid and dashed curves are respectively for best fitting Gaussian models and for a 0.7 arcsec source. Bottom row : Weak scattering spectra for elongations 45–50°. Solid and dashed curves are for 0.2 and 0.7 arcsec sources. Dashed horizontal lines show the r.m.s. levels of the spectra at high frequencies (Coles & Kaufman 1977).

A pattern's anisotropy is determined not only by source effects—which can be predicted—but also by the properties of the solar wind. For instance, the strength of turbulence determines the apparent axial ratio of an elliptical source, which will appear more nearly circular when the scintillation spectrum cuts off earlier than the source visibility function (*i.e.* in weak scattering). Furthermore the electron density irregularities themselves may also be anisotropic. Spacecraft measurements show that these tend to be aligned along the direction of the local magnetic field, but they vary sufficiently so that their overall effect on the scintillation pattern is, for purposes of estimating the velocity, unpredictable.

The direction of flow of the solar wind, on the other hand, is well known to be highly radial beyond a distance of a few solar radii from the sun. Spacecraft measurements find flow angle distributions with typical widths less than 3° (Mihalov & Wolfe 1971). Thus any large execursion from the radial in the flow angle measured in an IPS experiment of high signal-to-noise ratio should be attributed to an anisotropic pattern, and the velocity magnitude should be calculated under the assumption of radial flow.

5. The 3-dimensional solar wind

5.1 *Calibration of ecliptic IPS velocity using in situ spacecraft measurement*

In the ecliptic, the solar wind velocity estimate provided by IPS is only a crude and difficult-to-interpret version of a parameter which can be more accurately measured by spacecraft. One might argue that IPS is more cost-effective and that it can usually provide more simultaneous samples of the ecliptic wind, but for most purposes spacecraft observations are superior. Space crafts, however, have the serious limitation that they are confined to the ecliptic because of energy considerations, whereas IPS can monitor the solar wind over the entire sky. This makes it useful, and necessary to calibrate the ecliptic IPS data and infer the distribution of electron density fluctuations (Δn_e) that cause IPS. A detailed study of this kind has been made by comparing the IPS velocity data from the ecliptic radio source 3C144 with the IMP 6, 7, 8 spacecraft data during the period 1973–75 (Ananthakrishnan *et al.* 1980). The derived prototype distribution of Δn_e shows a close relation with the velocity structure of the solar wind stream rather than with proton density n_p. In an earlier paper by Houminer & Hewish (1974) a strong correlation was shown to be present between scintillation index m (where $m \propto \Delta n_e$) and n_p, but no quantitative estimates were given. But the detailed quantitative analysis on a much larger data base by Ananthakrishnan *et al.* (1980) shows that the correlation coefficients between observed and model velocities are 72 per cent and 47 per cent respectively for the derived model for Δn_e and for the $\Delta n_e \propto n_p$ model. Similarly the correlation coefficients between obser ved and model scintillation indices are 68 per cent and 40 per cent. These results indicate that the derived prototype distribution of Δn_e provides a much better approximation for the distribution of electron density fluctuations than the proton density. In figure 5a are shown the average profiles for the proton velocity V_p, the proton density n_p and the derived prototype distribution of electron density fluctuations. It is seen that Δn_e attains a maximum nearly twice its average value, *12 hours after the density peak.* It slowly decays inside the stream lasting for about 4 days. This is in marked contrast to the well known profile of n_p

which has a sharp rise and fall followed by a region of rarefaction lasting several days as shown in figure 5a.

This is further illustrated in figure 5b where the epoch average Δn_e profile is compared with epoch averages of other plasma paramters namely proton density n_p, proton temperature T_p, magnetic field fluctuations σ_B and the positive velocity gradient ΔV^+ for two groups of velocity streams divided according to their widths. The broader streams have more complex internal velocity structure than the narrow streams. The derived Δn_e profile for both cases has been overplotted on other parameters for easy comparison. It is clear that the closest match to the Δn_e profile over small as well as large time scales is given by ΔV^+ to which a constant has been added and to a lesser extent by σ_B. Thus Δn_e is not strongly correlated with n_p but appears to be enhanced in regions where high-speed wind is overtaking slow-speed wind. Such enhancements in Δn_e may be caused by processes unique to regions of increasing velocity, or may simply reflect the local amplification of processes taking place everywhere. Further, it is possible that Δn_e is connected to a particular type of field activity (*e.g.* fluctuations due to hydromagnetic waves) because of its good correlation with σ_B. More observations as well

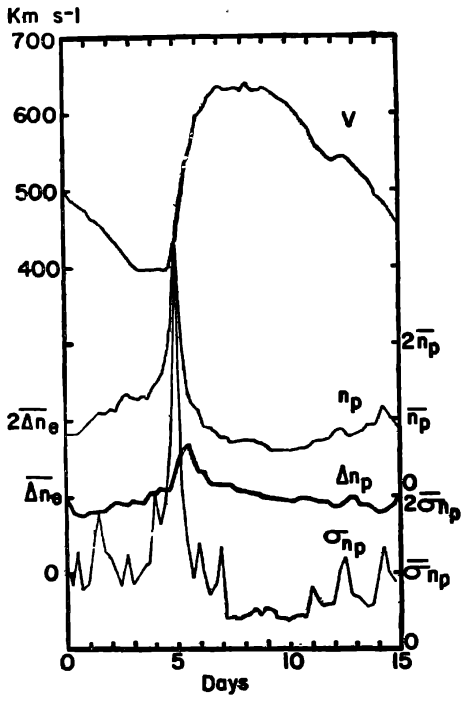

Figure 5a. Epoch average profiles for proton velocity V, proton density n_p, derived prototype distribution model for Δn_e, low frequency proton density fluctuation σ_{n_p} . σ_{n_p} is an average of 8 streams; the others are averages of 23 streams. Each parameter (except V) is normalized so that one division is equal to the parameter's mean value, denoted by a bar. Scales have offset zeroes and alternate from side to side (Ananthakrishnan *et al.* 1980).

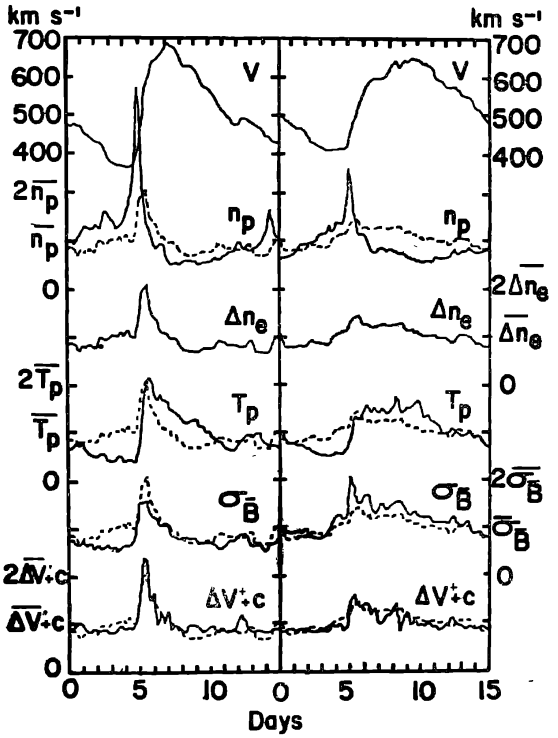

Figure 5b. Epoch average profiles for narrow and broad streams, showing the proton velocity V, the proton density n_p, derived model for Δn_e, proton temperature T_p, low frequency magnetic field fluctuations σ_B and the positive velocity gradient ΔV^+, to which a constant, c, has been added. Δn_e model has been overplotted (dashed lines) on the other parameters (except V). Other details are as in figure 5a (Ananthakrishnan *et al.* 1980).

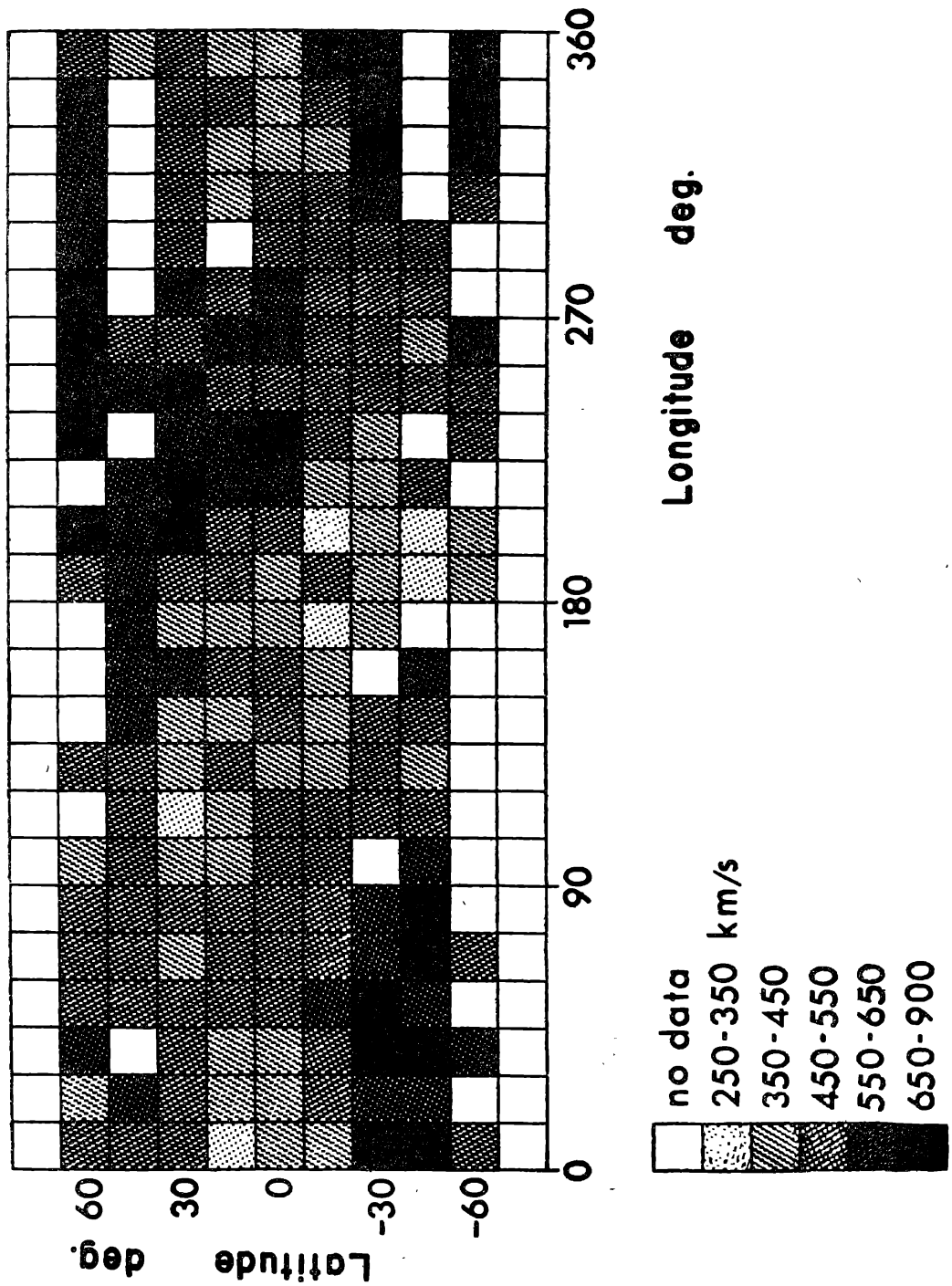

Figure 6. The average solar wind speed in 15° × 15° bins of heliographic latitude and longitude coded by grey scales as indicated. The IPS data were averaged for carrington rotations 1612 – 1617 (1974 March–July) (Coles *et al.* 1980).

as detailed analysis and modelling will be required to get a better insight into this interesting problem of interrelationship between Δn_e, ΔV^+ and σ_B. In any case, with the prototype distribution Δn_e thus obtained, it is now possible to extrapolate and infer the velocity structure more accurately at high heliographic latitudes not covered by spacecraft. This is now being attempted by the San Diego group.

5.2 *Polar solar wind*

Although an accurate description of the global velocity structure by the method of IPS requires a clear understanding of the prototype distribution Δn_e in the higher latitudes the work so far indicates that the speed observed by IPS is within ± 50 km s^{-1} of the solar wind speed at the point where the radio wave scattering is strongest. We may thus adopt the simplified inerpretation that the IPS speed gives an estimate of the solar wind speed at that single point in space. By observing the IPS of several radio sources daily and obtaining solar wind speed estimates at 3–5 locations at different heliographic latitudes it is possible to produce an averaged velocity map of the sun. Such a map is shown in figure 6 (Coles *et al.* 1980) for the averaged data from four solar rotations during which the configuration of the corona was relatively unchanged.

It is informative to compare the variations in the solar wind as given in figure 6 with high latitude activity seen in a variety of photospheric and lower coronal observables. One such observable is the interensity of scattered white light in the lower corona, as measured by K-coronameter, shown in contour map of figure 7. The contour chosen is thought to be a good indicator of 'coronal holes'—large stable regions of decreased particle density. From this comparison, it is evident that the higher velocity wind (denoted by the darker shadings) originates most often from the coronal hole regions. Such comparisons have established beyond doubt the global association of high velocities with coronal holes, just as spacecraft observations previously established their connection in the ecliptic.

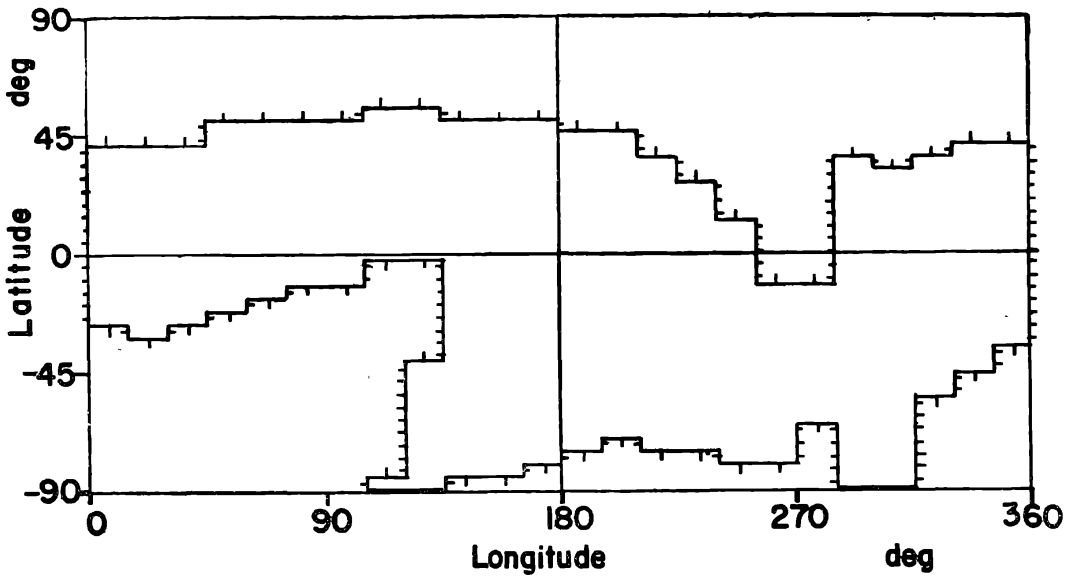

Figure 7. Coronal holes indicated by a contour of low K-coronameter polarization brightness (1.5 × 10 pB); the tick marks point towards low brightness, that is, towards the holes. Data supplied by Hansen are averaged for the same period as in figure 6 (Coles *et al.* 1980).

It is the study of such connections that makes multi-station observations of IPS an important tool in solar physics. As more and more data are accumulated, investigators are beginning to study long-term trends—variations within the ll-year solar cycle and differences from cycle to cycle. The completion of the new Indian multi-station IPS observatory will enhance the ability of investigators to resolve rapid time changes and examine complex spatial variations in the velocity structure of the solar wind. With the availability of observations from three widely separated systems—in India, Japan and U.S.A.—the study of transient disturbances becomes more feasible. Simultaneous observations with spacecraft during the planned solar-polar mission will provide a rich body of new data which may significantly enhance our understanding of the solar wind on a global scale.

Acknowledgements

The authors thank Prof. B. J. Rickett and Dr V. K. Kapahi for their critical reading of the manuscript and helpful suggestions. S.A. thanks IAU Commission 38 for a travel grant to go to San Diego, where most of this work was done.

References

Alurkar, S. K. & Bhonsle, R. V. (1980) *IAU Symp. No. 91*, p. 405.
Ananthakrishnan, S. (1976) *Ph.D. thesis*, University of Bombay.
Ananthakrishnan, S., Coles, W. A. & Kaufman, J. J. (1980) *J. Geophys. Res.* **85**, 6025.
Armstrong, J. W. (1975) *Ph.D. thesis*, University of California, San Diego.
Armstrong, J. W. & Coles, W. A. (1972) *J. Geophys. Res.* **77**, 4062.
Cohen, M. H. (1969) *A. Rev. Astr. Ap.* **7**, 619.
Coles, W. A. & Maagoe, S. (1972) *J. Geophys. Res.* **77**, 1105.
Coles, W. A. & Kaufman, J. J. (1977) *M. N. R. A. S.* **181**, 57.
Coles, W. A. & Kaufman, J. J. (1978) *Radio Sci.* **13**, 591.
Coles, W. A. (1978) *Sp. Sci. Rev.* **21**, 411.
Coles, W. A. *et al.* (1980) *Nature* **286**, 239.
Dennison, P. A. & Hewish, A. (1967) *Nature* **213**, 343.
Hewish, A., Scott, P. F. & Wills, D. (1964) *Nature* **203**, 1214.
Houminer, Z. & Hewish, A. (1974) *Planet. Sp. Sci.* **22**, 1041.
Kaufman, J. J. (1976) *Ph.D. thesis*, University of California, San Diego.
Little, L. T. & Ekers, R. D. (1971) *Astr. Ap.* **10**, 306.
Mihalov, J. D. & Wolfe, J. H. (1971) *Cosmic Electrodyn.* **2**, 326.
Parker, E. N. (1958) *Ap. J.* **128**, 664.
Sime, D. G. (1976) *Ph.D. thesis*, University of California, San Diego.
Swarup. G. (1977) *J. Sci. Ind. Res.* **36**, 569.
Vitkevich, V. V. & Vlasov, V. I. (1970). *Sov. Astr. A. J.* **13**, 669.
Watanabe, T., Kakinuma, T., Kojma, M. & Shibasaki, K. (1973) *J. Geophys. Res.* **78**, 8364.
Woo, R. & Armstrong, J. W. (1979) *J. Geophys. Res.* **84**, 7288.